

Coherent vibrational dynamics of NbO₂ filmYuhan Wang,^{1,2} Zhonghui Nie,³ Yongliang Shi,⁴ Yue Wang^{3,*} and Fengqiu Wang^{1,2,†}¹*School of Electronic Science and Engineering and Collaborative Innovation Center of Advanced Microstructures, Nanjing University, Nanjing 210093, China*²*Key Laboratory of Intelligent Optical Sensing and Manipulation, Ministry of Education, Nanjing University, Nanjing 210093, China*³*MIT Key Laboratory of Advanced Display Materials and Devices, Institute of Optoelectronics and Nanomaterials, College of Materials Science and Engineering, Nanjing University of Science and Technology, Nanjing 210094, China*⁴*Center for Spintronics and Quantum Systems, State Key Laboratory for Mechanical Behavior of Materials, School of Materials Science and Engineering, Xi'an Jiaotong University, Xi'an 710049, China*

(Received 4 September 2021; accepted 7 March 2022; published 31 March 2022)

The high thermodynamic transition temperature (≈ 1080 K) of niobium dioxide (NbO₂) makes it advantageous in differentiating the effects of electronic excitation and heat accumulation in the photoinduced phase transition. Recently, a photoinduced nonthermal metallization of NbO₂ film has been claimed [R. Rana, J. M. Klopff, J. Grenzer, H. Schneider, M. Helm, and A. Pashkin, *Phys. Rev. B* **99**, 041102(R) (2019)], but the simultaneous lattice evolution still remains blank. In this paper, photoinduced evolution in lattice vibrations of a crystalline NbO₂ film has been investigated using broadband coherent phonon spectroscopy. Signatures of two optical phonons at 155 and 185 cm⁻¹ are identified, and the corresponding lattice vibrations are found to be associated with the motions of Nb-Nb dimers. Pump fluence-dependent measurements reveal an electronic phase transition at a threshold fluence of ≈ 10 mJ/cm², while the lattice structure is preserved. A transient disordering in the lattice vibration is simultaneously observed, but lattice transformation is prevented probably by the large enthalpy barrier of the strong Peierls insulation. The accompanied drastic modulation in optical properties without atomic rearrangement also suggests the potential of NbO₂ in improving the operation speed of related devices.

DOI: [10.1103/PhysRevMaterials.6.035005](https://doi.org/10.1103/PhysRevMaterials.6.035005)

I. INTRODUCTION

Understanding and manipulating the complex phase transition phenomena in strongly correlated oxides are among the most important issues in condensed matter physics, with both fundamental and technological implications. Vanadium dioxide (VO₂), as one of the most studied materials, undergoes an insulator-metal transition (IMT) and a crystallographic phase transition (CPT) at ≈ 340 K [1,2]. The simultaneous transformations in electronic and lattice structures complicate the nature of the IMT, which has been attributed to the collaborative efforts of electron-electron correlation (Mott mechanism) [3] and electron-lattice interaction (Peierls mechanism) [4,5]. By probing the temporal evolution of the charge and lattice degrees of freedom, time-resolved studies on the photoinduced phase transition of VO₂ promise opportunities to disentangle these two coupled mechanisms. However, owing to its low thermodynamic transition temperature, it is rather challenging to discriminate the effects of photoexcitation and heating, making it still controversial on whether a metallic state with a monoclinic lattice can be obtained within a certain range of excitation fluences, i.e., whether the electronic correlation

(Mott insulation) can be melted alone without breaking the V-V dimerization [6].

Niobium dioxide (NbO₂) is a 4d¹ isovalent of VO₂ and exhibits similar phase transition at a much higher temperature (≈ 1080 K), between a body-centered tetragonal (bct, space group *I4₁/a*) semiconducting phase and a regular rutile (space group *P4₂/mmm*) metallic one [7,8]. Both NbO₂ and VO₂ have one *d* electron not engaged in the metal-oxygen bonding, and their local lattice distortion at the CPT is essentially the same: pairing of the metal ions along the rutile *c* (*c_R*) axis and tilting with respect to the *c_R* axis [5,9]. As the 4d electrons of NbO₂ are more dispersed (in both space and energy) than the 3d ones of VO₂, the electronic correlation is expected to be weaker than that of VO₂. Meanwhile, the larger overlap of 4d orbitals within the Nb-Nb dimers could strengthen the intradimer bonds and consequently lead to stronger Peierls insulation [10,11]. The high transition temperature of NbO₂ makes it less susceptible to the thermally driven phase transition, thus suitable to be studied to disentangle the evolution of electronic and lattice subsystems during the photoinduced phase transition. Recently, photoinduced metallization of NbO₂ has been demonstrated by terahertz spectroscopy [12,13], and claimed to be nonthermal based on the estimated photoinduced heating [12]. Meanwhile, a better understanding on its phase transition physics would still need information on the evolution of the lattice degree of freedom, which has been barely studied.

*ywang@njust.edu.cn

†fwang@nju.edu.cn

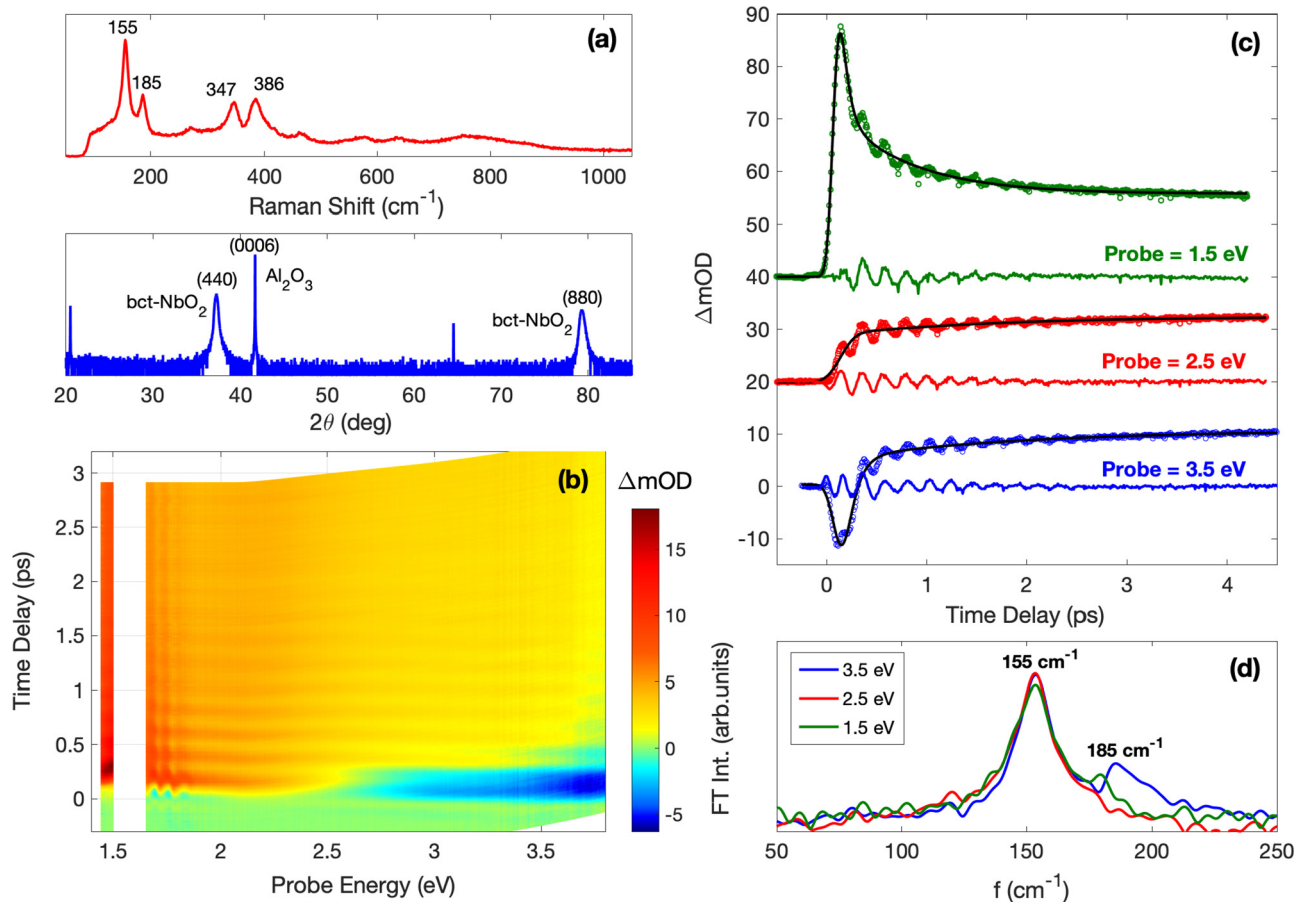


FIG. 1. Coherent phonons of NbO₂ films. (a) Raman spectrum under 514-nm excitation (top) and x-ray 2θ scan of the NbO₂ film grown on a sapphire (0001) substrate (bottom). (b) Broadband TA spectrum of the NbO₂ film under a 1.55-eV (800-nm) pump with a fluence of $\approx 1.6 \text{ mJ/cm}^2$. (c) Probe energy-dependent cuts of the spectrum in panel (b) at probe energy $\approx 3.5 \text{ eV}$ (350 nm), $\approx 2.5 \text{ eV}$ (500 nm), and $\approx 1.5 \text{ eV}$ (830 nm). Colored circles represent experimental data and black lines show the fitted population dynamics. Colored solid lines show the oscillatory components due to the modulation by coherent phonons. (d) FT spectra of the oscillatory components in panel (c), exhibiting coherent phonons peaks at ≈ 155 and $\approx 185 \text{ cm}^{-1}$ (at probe energy $\approx 3.5 \text{ eV}$).

Among various time-resolved spectroscopy techniques, coherent phonon spectroscopy using a broadband optical probe is capable of simultaneously sensing the temporal evolution of lattice and electronic changes, maintaining the consistency when comparing the pump fluence dependence of these two subsystems [14,15]. In the present paper, we adopt this method to investigate coherent lattice vibrations in a crystalline NbO₂ film and their evolution under intense photoexcitation. Two optical coherent phonon modes are observed at ≈ 155 and $\approx 185 \text{ cm}^{-1}$, which are related to the Nb atoms' motions within the dimers and couple with the $d_{||}-e_g^{\pi}$ and $d_{||}-d_{||}^*$ orbital splittings. When the pump fluence exceeds a threshold value at $\approx 10 \text{ mJ/cm}^2$, a transition in electronic structure is induced without initiating the lattice rearrangement, which also coincides with a transient disordering in the lattice vibration. NbO₂ is thus proved to be an ideal choice for understanding the role played by the lattice degree of freedom in the phase transitions of strongly correlated oxides.

II. SAMPLE CHARACTERIZATION

The NbO₂ film was deposited on a *c*-plane sapphire substrate by reactive bias target ion beam deposition.

Detailed growth procedures and conditions have been reported elsewhere [16]. The film thickness was determined by x-ray reflectivity to be $\approx 115 \text{ nm}$. Phase composition and microstructure of the film were characterized by Raman spectroscopy and x-ray diffraction 2θ scan, as shown in Fig. 1(a). The Raman spectrum demonstrates a good match with previously reported Raman spectra of bct-NbO₂ films [10,17–19]. In the x-ray diffraction 2θ scan, only two peaks from the film are observed at $2\theta = 37^\circ$ and 79° , which correspond to the (440) and (880) diffractions of bct-NbO₂. No Raman or x-ray diffraction peaks of other niobium oxide phases (NbO or Nb₂O₅) are observed. Hence it can be assumed that the studied film contains predominantly the semiconducting bct phase of NbO₂ with the (110)_{bct}/(100)_{rutile} orientation along the out-of-plane direction.

III. RESULTS

A. Coherent phonon modes in the NbO₂ film

The broadband transient absorption (TA) spectroscopy was conducted at room temperature with an 800-nm pump and a white light probe. A femtosecond amplified Ti:sapphire laser source (Solstice Ace) was employed to provide 100-fs

1-kHz pulses with central wavelength at 800 nm (1.55 eV). One part of the laser power was focused using a lens with ≈ 750 -mm focal length onto the sample surface, modulated by a mechanical chopper at 500 Hz. The rest of the laser was used to generate white light through a CaF₂ crystal plate, and the generated light was then focused onto the sample surface by an off-axis parabolic mirror. The spot sizes of the pump and probe beams were measured by a standard beam profiler, being ≈ 400 and ≈ 350 μm , respectively. The time delay between pump and probe beams was controlled by a motorized stage. The transient probe transmission was measured directly by a commercial spectrometer equipped with a silicon detector, so that the entire spectrum could be collected at each time delay. The chirp induced by the nonlinear process during the white light generation process has been corrected for all the experimental data. It should be noted that although there is a thin overoxidized Nb₂O₅ layer (≈ 1 nm) at the surface of the film [16], it should have negligible contribution to the measured TA signal due to its large band gap (above 3 eV, much larger than the pump energy 1.55 eV) [20].

Figure 1(b) shows the broadband TA spectrum of the NbO₂ film, measured under a pump fluence ≈ 3.6 mJ/cm² at room temperature. The blank regime near 1.5 eV is due to the saturation of the detector caused by the intense 800-nm laser used for the white light generation. The TA spectrum exhibits a negative peak for probe energy above 2.5 eV, and a strong positive peak just below probe energy 1.5 eV, which can be attributed to the photoinduced band gap shrinkage and band-filling effects [21]. More interestingly, a periodic modulation on the TA signal can be clearly found during the first several picoseconds, which is a typical feature of coherent lattice vibrations, known as coherent phonons [22]. The oscillatory feature of the TA spectrum is noticeable across the whole probed energy range, indicating the broadband modulation by the coherent phonons on the electric susceptibility.

To identify the observed coherent phonon modes, the oscillatory components of the TA signal have been obtained by subtracting the incoherent background. Fittings to the nonoscillatory population dynamics of three exemplary TA curves at probe energy ≈ 1.5 eV (830 nm), ≈ 2.5 eV (500 nm), and ≈ 3.5 eV (350 nm) are displayed in Fig. 1(c), together with the extracted oscillatory components. By taking Fourier transformation (FT) of the residual oscillating signals, frequency spectra at different probe wavelengths can be obtained. As shown in Fig. 1(d), a prominent peak at ≈ 155 cm⁻¹ and another weaker peak at ≈ 185 cm⁻¹ (for the signal probed at ≈ 3.5 eV) are present, matching well with the measured Raman peaks in Fig. 1(a). Such good agreement confirms that the oscillation in the TA spectrum arises from the Raman-active phonons of the NbO₂ film. The independence of phonon frequencies on the probe energy also indicates that these phonons are optical phonons instead of acoustic ones [23].

Before using the coherent phonons behaviors' evolution as indicators of photoinduced lattice changes, specific vibrational modes corresponding to these two phonons, as well as their coupling with different electronic orbital splittings, need to be clarified. For this purpose, the phonon modes and electronic band structure of bct-NbO₂ have been calculated (calculation details in Note I of Supplemental Material [24]). The calculation yields several vibrational modes at

the Γ point with frequencies close to those of the observed phonons, as listed in Table SI of Supplemental Material [24]. Since only Raman-active coherent phonons can be resolved by pump-probe spectroscopy [22], the observed coherent phonons should correspond to two or more modes with A_g , B_g , or E_g symmetry, as marked in Table SI of Supplemental Material [24]. Two peaks with similar frequencies are exhibited in the calculated Raman spectrum [Fig. 2(c)]. Further assignment to specific modes through phonon symmetry by polarization dependent measurements cannot be made, as the sample is polycrystalline.

Next, atomic motions of these Raman-active modes have been investigated. It was found that these modes mainly associate with the motion of Nb atoms, which is in line with the large difference in Nb and O atomic masses [25]. As is shown by Fig. S2 of Supplemental Material [24], the vibration of these modes can be seen as the relative motions of Nb atoms within the dimers, either stretching or tilting the Nb-Nb dimers with respect to the c_R direction. Comparing Figs. S2(a) and S2(b) of Supplemental Material [24], it is noticed that the Nb atoms' motions of the high-frequency modes exhibit much larger amplitudes. More importantly, while for the low-frequency modes (near 155 cm⁻¹) the displacements of Nb atoms are mostly perpendicular to the chains of Nb-Nb dimers, the high-frequency modes (near 185 cm⁻¹) all demonstrate large components along this direction. Figures 2(d) and 2(e) show detailed analysis on one example of each kind of mode, and it can be seen that the Nb-Nb distance along the c_R axis can be effectively modulated by the high-frequency one (by $\approx 6\%$).

To clarify the interaction of these two phonons with the electronic bands, dependence of the coherent phonon amplitude on the probe energy has been analyzed. As shown in Fig. 3(a), the 155-cm⁻¹ mode shows a $\approx 50\%$ amplitude variation across the probed energy range and a maximum value at probe energy ≈ 1.6 eV, while the 185-cm⁻¹ mode can only be distinguished from the background noise at a probe energy above 3 eV. Such dependence on the probe energy, as well as a π phase shift of the oscillatory TA signal corresponding to the 155-cm⁻¹ phonon near probe energy ≈ 1.6 eV [Fig. 3(b)], indicate that the 155- and 185-cm⁻¹ modes couple with two interband electronic transition resonances near ≈ 1.6 eV and above 3 eV. As is illustrated by the calculated projections of the density of states (DOS) to different orbitals in Fig. 3(c), these two orbital splittings correspond to the $d_{||}-e_g^\pi$ and $d_{||}-d_{||}^*$ resonances, respectively. More detailed analysis can be found in Note II of Supplemental Material [24]. Similar sizes of these two orbital splittings have also been determined experimentally by optical conductivity measurements on similar crystalline NbO₂ film samples [10]. Hence these two coherent phonons, which relate to the vibrations of Nb-Nb dimers and couple with $d_{||}-e_g^\pi$ and $d_{||}-d_{||}^*$ orbital splittings, should be useful in resolving the photoinduced evolution in the lattice structure and deciphering its relation with potential changes in electronic structures.

B. Nonthermal phase transition without lattice transformation

To explore possible occurrence of photoinduced transitions in lattice and/or electronic subsystems, broadband TA spectra

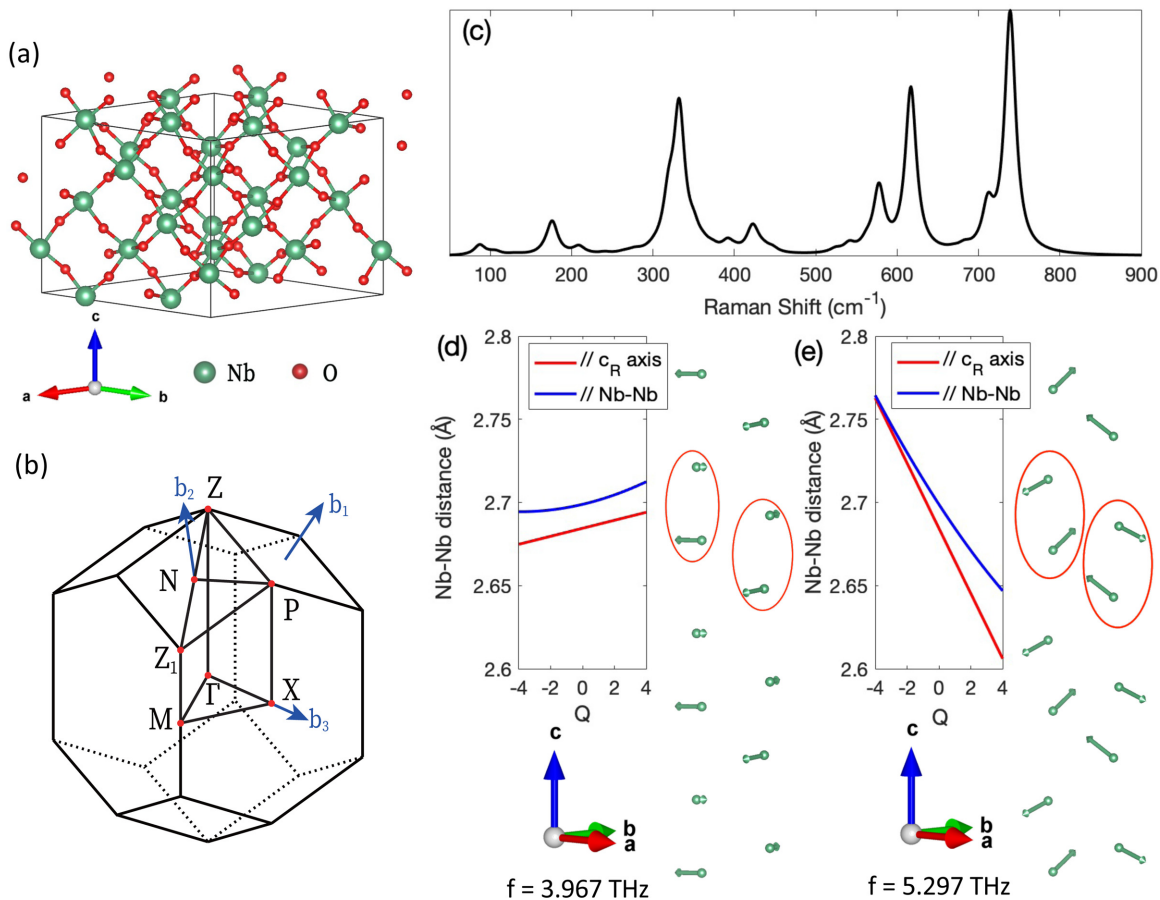


FIG. 2. Theoretical calculation on the lattice vibrations of bct-NbO₂. (a, b) Crystal structure of the primitive cell (a) and the Brillouin zone (b) of bct-NbO₂ used in the calculation. (c) Calculated Raman spectrum of the bct-NbO₂. Diagrammatic representations of the calculated vibrational modes corresponding to the observed coherent phonons with frequencies close to the (d) 155- and (e) 185-cm⁻¹ coherent phonons. The insets show the modulation of Nb-Nb distance within the dimers caused by the respective lattice vibrations.

under gradually increased pump fluences have been measured. The static transmission was checked after each scan, to make sure that the sample had fully recovered. Irreversible changes were observed after scanning with pump fluence ≈ 14.4 mJ/cm².

Analysis on the pump fluence dependence of coherent phonon behaviors has been conducted mainly using the TA signals at probe energy ≈ 3.5 eV (350 nm). First, the oscillation in TA signals have remained observable in all scans up to the damage threshold [Fig. 4(a)]. Next, the frequencies and amplitudes of corresponding peaks in FT spectra have been extracted and plotted as functions of pump fluence [Figs. 4(b) and 4(c)]. Frequencies of both phonon modes remain relatively constant against the variation of pump fluence, suggesting that the lattice transformation has not been initiated. Under relatively weak photoexcitation, the amplitudes of both phonons increase almost linearly with the pump fluence. When the pump fluence exceeds a threshold (F_{th}) of ≈ 10 mJ/cm², the phonon amplitudes start to deviate from the linear dependence. The 155-cm⁻¹ mode demonstrates a saturation of the amplitude. For the 185-cm⁻¹ mode, despite the enhanced uncertainty of the phonon amplitude extraction, it can still be seen that the corresponding lattice vibration experiences a suppression above the threshold fluence F_{th} .

Within the perturbation regime, the amplitude of coherent phonons in absorbing media should depend on the photoexcited carrier density [26–28]. To exclude possible effects from nonlinear absorption (e.g., saturable absorption and two-photon absorption), the fluence-dependent absorption of the NbO₂ film at pump wavelength 800 nm has been measured (Fig. S5 of Supplemental Material [24]), which could be deemed to be nearly constant within the measured fluence range. Although there is a slight reduction of absorption near the damage threshold, such variation of absorption cannot account for the observed nonlinearity of phonon amplitudes at F_{th} . In addition, we also extracted the maxima of TA signals at probe energy ≈ 3.5 eV (350 nm) and ≈ 1.5 eV (830 nm), which exhibit nearly linear dependence on the pump fluence up to the damage threshold (Fig. S6 of Supplemental Material [24]). Hence the nonlinear absorption can be excluded as the origin of the nonlinearity at F_{th} . On the other hand, assuming that the absorbed photon energy can fully convert to lattice heating, the upper limit of the photoinduced lattice temperature rise is estimated to be ≈ 26.4 K for 1-mJ/cm² optical excitation (details in Note III of Supplemental Material [24]). As the heat capacity of NbO₂ only experiences a steady and limited increase within the largest possible range of photoinduced temperature rise [29], no abrupt changes in lattice temperature with the increase of pump intensity are expected. With the

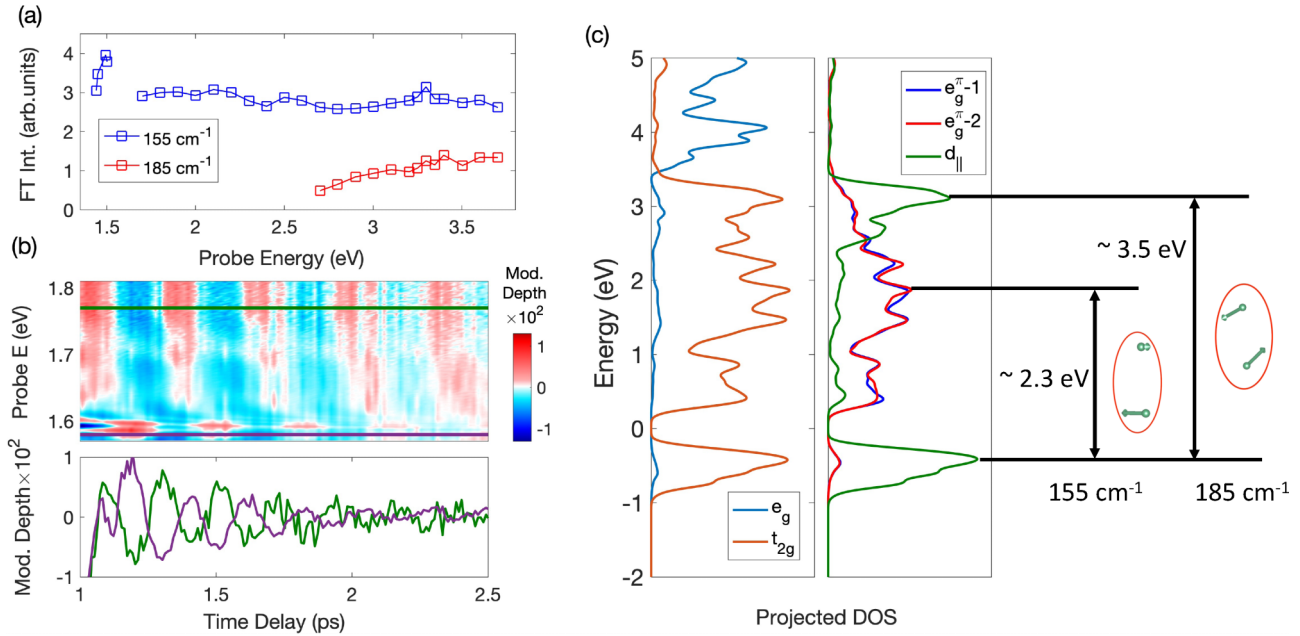


FIG. 3. Lattice vibrations corresponding to the coherent phonons. (a) Amplitudes of the coherent phonons (characterized by the FT intensity) as functions of the probe energy. (b) Oscillatory components of the TA spectra excited by an 800-nm pump at $\approx 1.6 \text{ mJ/cm}^2$ covering the probe energy from 1.57 to 1.8 eV (top) and probe energy-dependent cuts of the top panel at 1.58 and 1.77 eV (bottom), showing a π phase shift with respect to each other. (c) The projection of DOS to different orbitals of bct-NbO₂ and illustration of the coupling with the observed coherent phonons.

nonlinear optical absorption and lattice temperature rise being excluded, the changes in coherent phonon behaviors beyond F_{th} should arise from certain qualitative transitions of the sample. More importantly, it should be noted that the absorbed energy at F_{th} is far from enough to trigger the phase transition of NbO₂ thermally (i.e., bring the sample to $\approx 1080 \text{ K}$), thus this transition should be a nonthermal one.

Besides the coherent lattice vibration, nonlinear features near F_{th} have also been observed in the nonoscillating transient signals over a wide range of wavelengths. In Fig. 4(d) and Fig. S7 of Supplemental Material [24], the pump fluence dependence of the TA signal probed at $\approx 1.5 \text{ eV}$ (830 nm) and $\approx 3.5 \text{ eV}$ (350 nm) at the delay time of 1.5 ps has been analyzed, and inflection points can be found near F_{th} , suggesting abrupt changes of electronic band structure. More prominent switching can be observed at longer wavelengths. Figure S8 of Supplemental Material [24] shows the measured TA spectra in the mid-IR range (at $6 \mu\text{m}$), the energy ($\approx 0.2 \text{ eV}$) of which is much smaller than the band gap of the semiconducting NbO₂ (above 0.7 eV) [30–32]. By extracting transient peak amplitude at various fluences [shown in Fig. 4(e)], it is found that the transient signal at $\approx 0.2 \text{ eV}$ starts to surge at a fluence quite close to F_{th} , implying a sudden shrinkage or collapse of the band gap.

It has been demonstrated by theoretical calculation that although not as strong as in the VO₂ case, charge carriers in NbO₂ also experience electronic correlation and are close to the Mott transition [33]. The photocarrier density at F_{th} is estimated to be $\approx 3 \times 10^{20}/\text{cm}^3$, corresponding to ≈ 0.1 carrier per NbO₂ formula unit (calculation details can be found in Note IV of Supplemental Material [24]), which is beyond the

critical carrier density needed to trigger the Mott transition of NbO₂ ($1/32$ per NbO₂ formula unit) predicted by a recent density functional theory simulation study [34]. Hence what occurs at F_{th} here should be a certain transition in electronic structure driven by high-density electronic excitation. This observation agrees with the recent optical pump terahertz probe study claiming a subpicosecond formation of the metastable metallic state at the same pump fluence $\approx 10 \text{ mJ/cm}^2$ [12], and the preserved coherent phonon features further confirm that lattice transformation (Peierls transition) is not involved.

C. Temporal evolution of the coherent lattice vibration

It should be noted that the FT analysis is conducted by averaging over a certain time window. To further understand the anomalies in coherent phonon behaviors at F_{th} , the continuous wavelet transform (CWT) analysis has been performed to resolve the temporal evolution of the coherent lattice vibrations [35]. Figure 5(a) shows the CWT chronogram under a relatively low pump fluence ($\approx 4.8 \text{ mJ/cm}^2$), where the 155-cm^{-1} phonon mode exhibits a longer lifetime than the 185-cm^{-1} one does. Moreover, the two phonons' frequencies have been extracted from a series of temporal cuts, and the temporal evolution is given in Fig. 5(b). The frequency of the 155-cm^{-1} mode is nearly independent of the delay time. In contrast, strongly anharmonic behaviors are found in the 185-cm^{-1} mode, where its frequency drops abruptly upon photoexcitation and then gradually recovers within $\approx 1.5 \text{ ps}$.

The transient softening of the coherent phonon indicates changes in the curvature of the lattice potential, caused by photoexcitation [14]. As is shown before, the atomic motion

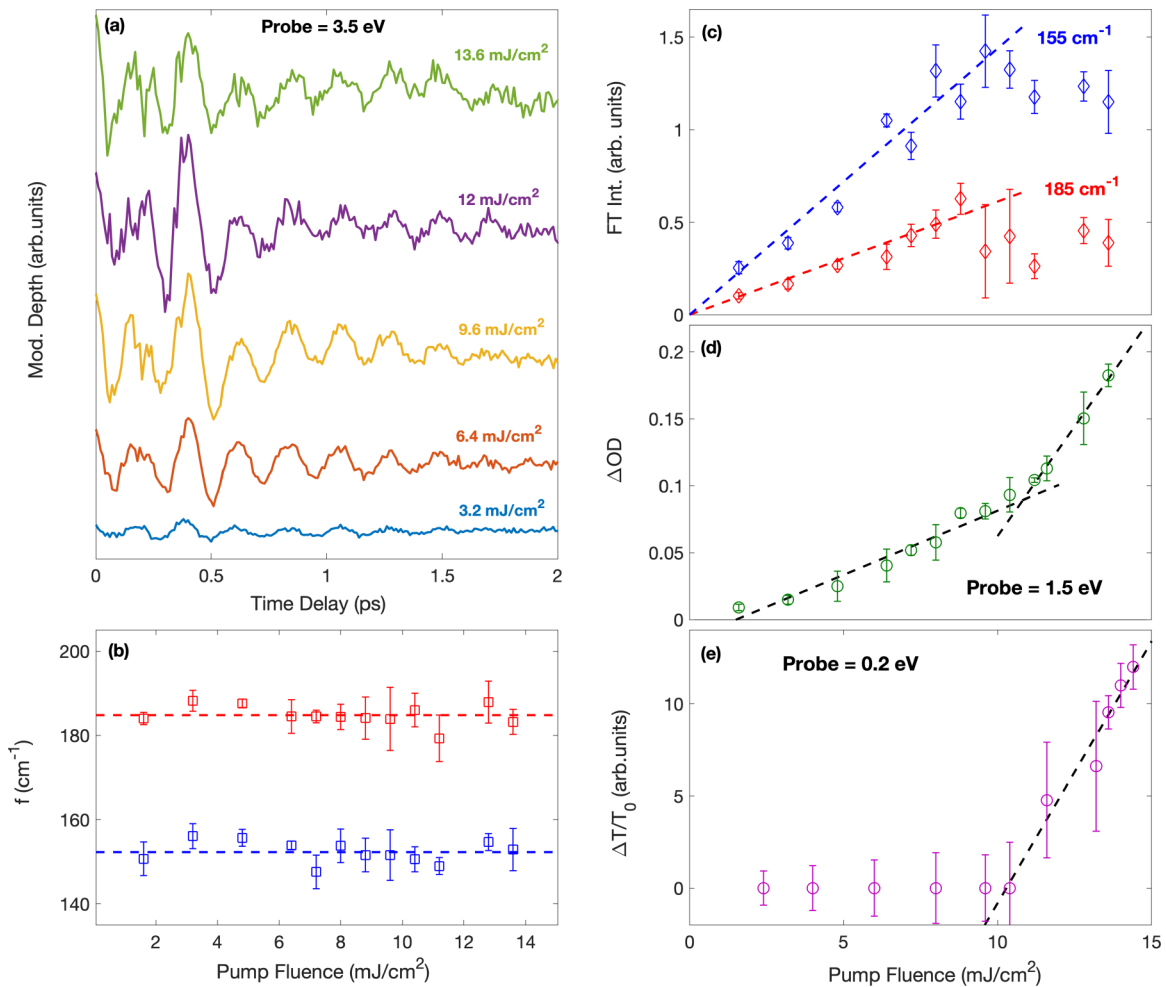


FIG. 4. Pump fluence dependences of coherent lattice vibrations and optical responses. (a) Oscillatory components of TA signals at probe energy ≈ 3.5 eV under different pump fluences. (b, c) Phonon frequencies (b) and amplitudes (c) extracted from FT spectra. (d) TA amplitude at 1.5 ps probed at ≈ 1.5 eV (830 nm) as a function of pump fluence. (e) Extracted peak amplitude of the differential transmission ($\Delta T/T_0$) probed at $6 \mu\text{m}$ (≈ 0.2 eV) as a function of pump fluence.

represented by the 185-cm^{-1} mode has a large projection along the lattice distortion between the two phases of NbO_2 . Considering the Peierls distortion between the two phases with rutile and bct lattices, a phenomenological double-well potential $V(x, t)$ based on Ginzburg-Landau theory, with photoinduced modulation, has been employed to understand the transient behaviors of the 185-cm^{-1} mode [36]:

$$V(x, t) = V_0 + \frac{a}{2} \left[g \exp\left(-\frac{t}{\tau_{\text{disp}}}\right) - 1 \right] x^2 + \frac{b}{4} x^4 \quad (1)$$

where x represents the atomic coordinate along the lattice distortion between the rutile and bct- NbO_2 lattices and the term $g \exp(-\frac{t}{\tau_{\text{disp}}})$ represents the photoexcitation influence (g and τ_{disp} are related to pump fluence and photocarrier carrier decay). As is shown in Fig. S9(b) of Supplemental Material [24], the transient softening and recovery process of the 185-cm^{-1} mode after photoexcitation can be qualitatively reproduced (detailed calculation process and discussion can be found in Note V of Supplemental Material [24]).

Such photoinduced modulation on the lattice potential could originate from electronic softening, or phonon-phonon

interaction (lattice anharmonicity) [37]. It is noticed that the timescale of the recovery process of the 185-cm^{-1} mode's frequency is close to a many-body, Auger-like decay component in the nonoscillating TA spectra (see Fig. S11 of Supplemental Material [24] and [38,39]), suggesting that the photoexcitation of charge carriers may have a major contribution to this modulation effect. As the valence band maximum states are primarily involved in the Nb-Nb bonding along the c_R axis [see Fig. 3(c)], removing electrons from these states can effectively weaken the bonds and change the lattice potential along this direction. Hence the oscillation of the 185-cm^{-1} modes is expected to be influenced more severely than that of the 155-cm^{-1} mode, as its atomic motion has a much larger projection along the c_R axis.

When the pump fluence approaches and exceeds F_{th} , the lifetime of the 185-cm^{-1} mode decreases further, and a broad continuum signal starts to emerge near the 185-cm^{-1} mode [Figs. 5(c) and 5(d)], indicating that the lattice vibration is allowed over a wide range of frequencies instead of a well-defined one. Such phenomenon implies a greatly enhanced dephasing/damping of coherent lattice vibration, where the energy is quickly distributed within the system due to efficient

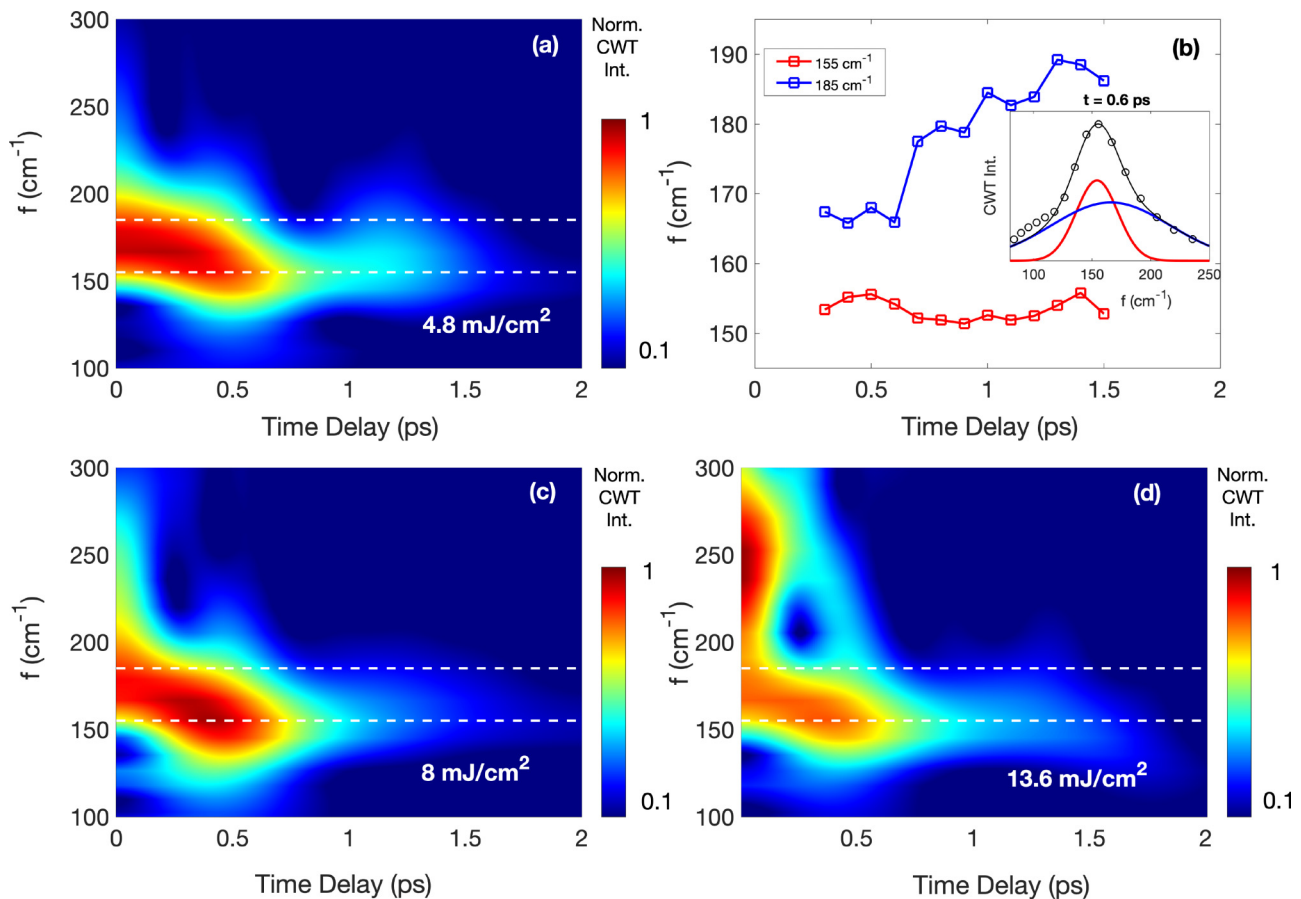


FIG. 5. Temporal evolution of the lattice vibration. CWT chronograms of oscillatory TA signals probed at ≈ 3.5 eV, under excitation fluence (a) ≈ 4.8 mJ/cm², (c) ≈ 8 mJ/cm², and (d) ≈ 13.6 mJ/cm². The white dashed lines mark the frequencies of 155 and 185 cm⁻¹ for reference. (b) Frequencies of coherent phonons as functions of delay time under pump fluence ≈ 4.8 mJ/cm². The inset illustrates the estimation of phonon frequencies from the temporal cuts of panel (a).

interaction with high-density carriers or other phonon modes [40].

The disordering of lattice vibration implied by the well-spread CWT signal resembles the recently reported photoinduced atomic disordering of VO₂ [41]. The resulting gain in phonon entropy has been shown to play an important role in stabilizing the rutile lattice of VO₂ [41,42]. Interestingly, unlike the case of VO₂, the rapid increase of phonon entropy in NbO₂ did not result in transformation to the rutile lattice. As the relative stability of two phases is determined by the difference between their Gibbs free energies, including the contributions from both entropy and enthalpy, the absence of CPT in NbO₂ thus implies that the photoinduced entropy increase cannot compensate for the large enthalpy difference between the two lattice structures, agreeing with the strong Peierls-type insulation of NbO₂. Compared with phase transitions that involve lattice transformation, the capability to obtain the drastic modulation in optical responses without the assistance of the CPT indicates the potential of NbO₂ in the application of all-optical modulations with higher speed, as slower recovery processes after heat dissipation are not needed. Moreover, the electronic nature of transition, and the large gap between this transition and the structural one, could also help to explain the respective role of electrical doping and Joule heating upon electrical

stimulation, which is beneficial to the actively researched resistive random-access memory and neuromorphic networking applications [43,44].

IV. CONCLUSION

In summary, coherent lattice vibrations in NbO₂ thin film have been studied. The broadband TA spectra within the visible/near-IR range were found to be modulated by the coherent lattice vibrations of two Raman-active optical phonons at ≈ 155 and ≈ 185 cm⁻¹, which associate with the motions of Nb-Nb dimers and couple with the $d_{||}-e_g^\pi$ and $d_{||}-d_{||}^*$ orbital splittings across the Fermi level. Upon photoexcitation beyond a critical fluence at ≈ 10 mJ/cm², a metastable state with qualitatively altered electronic structure and preserved atomic arrangement has been generated, exhibiting abrupt changes in optical properties and an ultrafast disordering in the lattice vibration. The opportunity to selectively trigger a pure electronic transition also implies the potential of NbO₂ in improving the speed of optical/electrical modulation devices, by avoiding slower lattice transformation processes.

ACKNOWLEDGMENTS

F.W. acknowledges support from National Key Research and Development Program of China (Grant No.

2017YFA0206304, 2018YFB2200500), National Natural Science Foundation of China (Grant No. 61804074) and the “Jiangsu Shuangchuang Doctor” Program. Yue Wang acknowledges support from Natural Science Foundation of

Jiangsu Province (Grant No. BK20190446) and National Natural Science Foundation of China (Grant No. 11904172).

Yuhan Wang and Z.N. contributed equally to this work.

-
- [1] F. J. Morin, Oxides which Show a Metal-To-Insulator Transition at the Neel Temperature, *Phys. Rev. Lett.* **3**, 34 (1959).
- [2] S. Westman, I. Lindqvist, B. Sparrman, G. B. Nielsen, H. Nord, and A. Jart, Note on a phase transition in VO₂, *Acta Chem. Scand.* **15**, 217 (1961).
- [3] A. Zylbersztejn and N. F. Mott, Metal-insulator transition in vanadium dioxide, *Phys. Rev. B* **11**, 4383 (1975).
- [4] J. B. Goodenough, The two components of the crystallographic transition in VO₂, *J. Solid State Chem.* **3**, 490 (1971).
- [5] V. Eyert, The metal-insulator transitions of VO₂: A band theoretical approach, *Ann. Phys. (NY)* **11**, 650 (2002).
- [6] L. Vidas, D. Schick, E. Martínez, D. Perez-Salinas, A. Ramos-Álvarez, S. Cichy, S. Batlle-Porro, A. S. Johnson, K. A. Hallman, R. F. Haglund, and S. Wall, Does VO₂ Host a Transient Monoclinic Metallic Phase? *Phys. Rev. X* **10**, 031047 (2020).
- [7] A. A. Bolzan, C. Fong, B. J. Kennedy, and C. J. Howard, A powder neutron diffraction study of semiconducting and metallic niobium dioxide, *J. Solid State Chem.* **113**, 9 (1994).
- [8] R. F. Janninck and D. H. Whitmore, Electrical conductivity and thermoelectric power of niobium dioxide, *J. Phys. Chem. Solids* **27**, 1183 (1966).
- [9] A. K. Cheetham and C. N. R. Rao, A neutron diffraction study of niobium dioxide, *Acta Crystallogr., Sect. B* **32**, 1579 (1976).
- [10] F. J. Wong, N. Hong, and S. Ramanathan, Orbital splitting and optical conductivity of the insulating state of NbO₂, *Phys. Rev. B* **90**, 115135 (2014).
- [11] V. Eyert, The metal-insulator transition of NbO₂: An embedded Peierls instability, *Europhys. Lett.* **58**, 851 (2002).
- [12] R. Rana, J. M. Klopff, J. Grenzer, H. Schneider, M. Helm, and A. Pashkin, Nonthermal nature of photoinduced insulator-to-metal transition in NbO₂, *Phys. Rev. B* **99**, 041102(R) (2019).
- [13] Y. Wang, J. Zhang, Y. Ni, X. Chen, R. Mescall, T. Isaacs-Smith, R. B. Comes, S. Kittiwatanakul, S. A. Wolf, J. Lu, and M. Liu, Structural, transport, and ultrafast dynamic properties of V_{1-x}Nb_xO₂ thin films, *Phys. Rev. B* **99**, 245129 (2019).
- [14] S. Wall, D. Wegkamp, L. Foglia, K. Appavoo, J. Nag, R. F. Haglund, J. Stähler, and M. Wolf, Ultrafast changes in lattice symmetry probed by coherent phonons, *Nat. Commun.* **3**, 721 (2012).
- [15] S. Wall, L. Foglia, D. Wegkamp, K. Appavoo, J. Nag, R. F. Haglund, J. Stähler, and M. Wolf, Tracking the evolution of electronic and structural properties of VO₂ during the ultrafast photoinduced insulator-metal transition, *Phys. Rev. B* **87**, 115126 (2013).
- [16] Y. Wang, R. B. Comes, S. Kittiwatanakul, S. A. Wolf, and J. Lu, Epitaxial niobium dioxide thin films by reactive-biased target ion beam deposition, *J. Vac. Sci. Technol. A* **33**, 021516 (2015).
- [17] Y. Zhao, Z. Zhang, and Y. Lin, Optical and dielectric properties of a nanostructured NbO₂ thin film prepared by thermal oxidation, *J. Phys. D* **37**, 3392 (2004).
- [18] S. Lee, H. Yoon, I. Yoon, and B. Kim, Single crystalline NbO₂ nanowire synthesis by chemical vapor transport method, *Bull. Korean Chem. Soc.* **33**, 839 (2012).
- [19] S. Kim, J. Park, J. Woo, C. Cho, W. Lee, J. Shin, G. Choi, S. Park, D. Lee, B. H. Lee, and H. Hwang, Threshold-switching characteristics of a nanothin-NbO₂-layer-based Pt/NbO₂/Pt stack for use in cross-point-type resistive memories, *Microelectron. Eng.* **107**, 33 (2013).
- [20] C. Nico, T. Monteiro, and M. P. F. Graça, Niobium oxides and niobates physical properties: Review and prospects, *Prog. Mater. Sci.* **80**, 1 (2016).
- [21] J. K. Clark, Y.-L. Ho, H. Matsui, H. Tabata, and J.-J. Delaunay, Thresholdless behavior and linearity of the optically induced metallization of NbO₂, *Phys. Rev. Research* **1**, 033168 (2019).
- [22] K. Ishioka and O. V. Misochko, in *Progress in Ultrafast Intense Laser Science*, edited by K. Yamanouchi, A. Giuliotti, and K. Ledingham (Springer-Verlag, Berlin, 2010), Vol. 5, pp. 23–46.
- [23] C. Thomsen, H. T. Grahn, H. J. Maris, and J. Tauc, Surface generation and detection of phonons by picosecond light pulses, *Phys. Rev. B* **34**, 4129 (1986).
- [24] See Supplemental Material at <http://link.aps.org/supplemental/10.1103/PhysRevMaterials.6.035005> for the calculated phonon modes of bct-NbO₂ at the Γ point, the calculated electronic band structure of bct-NbO₂, diagrammatic representations of calculated phonon modes with frequencies close to 155 and 185 cm⁻¹, probe energy dependence of the FT spectra, static absorption spectrum and pump fluence dependence of absorption at 800 nm of the sample, pump fluence dependence of the TA maximum amplitudes and amplitudes at 1.5 ps, differential transmission spectra probed at 0.2 eV of the sample, simulation results on temporal evolution of the 185-cm⁻¹ mode’s frequency and the oscillatory TA signal, normalized TA spectra under a 800-nm pump and 830-nm probe, calculation process on the phonon modes and electronic band structure of bct-NbO₂, analysis on coupling of coherent phonons to electronic bands, the estimation process on the photoinduced lattice temperature rise and absorbed photon density, as well as the simulation process on the photoinduced transient changes in phonon frequency.
- [25] E. Arcangeletti, L. Baldassarre, D. Di Castro, S. Lupi, L. Malavasi, C. Marini, A. Perucchi, and P. Postorino, Evidence of a Pressure-Induced Metallization Process in Monoclinic VO₂, *Phys. Rev. Lett.* **98**, 196406 (2007).
- [26] H. J. Zeiger, J. Vidal, T. K. Cheng, E. P. Ippen, G. Dresselhaus, and M. S. Dresselhaus, Theory for dispersive excitation of coherent phonons, *Phys. Rev. B* **45**, 768 (1992).
- [27] R. Merlin, Generating coherent THz phonons with light pulses, *Solid State Commun.* **102**, 207 (1997).
- [28] T. E. Stevens, J. Kuhl, and R. Merlin, Coherent phonon generation and the two stimulated Raman tensors, *Phys. Rev. B* **65**, 144304 (2002).
- [29] K. T. Jacob, C. Shekhar, M. Vinay, and Y. Waseda, Thermo-

- dynamic properties of niobium oxides, *J. Chem. Eng. Data* **55**, 4854 (2010).
- [30] S. Nakao, H. Kamisaka, Y. Hirose, and T. Hasegawa, Structural, electrical, and optical properties of polycrystalline NbO₂ thin films grown on glass substrates by solid phase crystallization, *Phys. Status Solidi A* **214**, 1600604 (2017).
- [31] A. O'Hara, T. N. Nunley, A. B. Posadas, S. Zollner, and A. A. Demkov, Electronic and optical properties of NbO₂, *J. Appl. Phys.* **116**, 213705 (2014).
- [32] J. Stoeber, J. E. Boschker, S. Bin Anooz, M. Schmidbauer, P. Petrik, J. Schwarzkopf, M. Albrecht, and K. Irmscher, Approaching the high intrinsic electrical resistivity of NbO₂ in epitaxially grown films, *Appl. Phys. Lett.* **116**, 182103 (2020).
- [33] W. H. Brito, M. C. O. Aguiar, K. Haule, and G. Kotliar, Dynamic electronic correlation effects in NbO₂ as compared to VO₂, *Phys. Rev. B* **96**, 195102 (2017).
- [34] Y. Liu, H. Zhang, and X. Cheng, Sequential insulating-metal-insulating phase transition of NbO₂ by doping photoexcited carrier, *Comput. Mater. Sci.* **173**, 109434 (2020).
- [35] M. Hase, M. Kitajima, A. M. Constantinescu, and H. Petek, The birth of a quasiparticle in silicon observed in time–frequency space, *Nature (London)* **426**, 51 (2003).
- [36] L. D. Landau, E. M. Lifšic, E. M. Lifshitz, and L. Pitaevskii, *Statistical Physics: Theory of the Condensed State* (Butterworth-Heinemann, Oxford, 1980).
- [37] S. Fahy and D. A. Reis, Coherent Phonons: Electronic Softening or Anharmonicity? *Phys. Rev. Lett.* **93**, 109701 (2004).
- [38] A. R. Beattie, P. T. Landsberg, and H. Fröhlich, Auger effect in semiconductors, *Proc. R. Soc. Lond. A* **249**, 16 (1959).
- [39] V. I. Klimov, Multicarrier interactions in semiconductor nanocrystals in relation to the phenomena of Auger recombination and carrier multiplication, *Annu. Rev. Condens. Matter Phys.* **5**, 285 (2014).
- [40] M. Hase and M. Kitajima, Interaction of coherent phonons with defects and elementary excitations, *J. Phys.: Condens. Matter* **22**, 073201 (2010).
- [41] S. Wall, S. Yang, L. Vidas, M. Chollet, J. M. Glowina, M. Kozina, T. Katayama, T. Henighan, M. Jiang, T. A. Miller, D. A. Reis, L. A. Boatner, O. Delaire, and M. Trigo, Ultrafast disordering of vanadium dimers in photoexcited VO₂, *Science* **362**, 572 (2018).
- [42] J. D. Budai, J. Hong, M. E. Manley, E. D. Specht, C. W. Li, J. Z. Tischler, D. L. Abernathy, A. H. Said, B. M. Leu, L. A. Boatner, R. J. McQueeney, and O. Delaire, Metallization of vanadium dioxide driven by large phonon entropy, *Nature (London)* **515**, 535 (2014).
- [43] S. Kumar, R. S. Williams, and Z. Wang, Third-order nanocircuit elements for neuromorphic engineering, *Nature (London)* **585**, 518 (2020).
- [44] S. Kumar, Z. Wang, N. Davila, N. Kumari, K. J. Norris, X. Huang, J. P. Strachan, D. Vine, A. L. D. Kilcoyne, Y. Nishi, and R. S. Williams, Physical origins of current and temperature controlled negative differential resistances in NbO₂, *Nat. Commun.* **8**, 658 (2017).